INTELSAT IV IN-ORBIT LIQUID SLOSH TESTS AND PROBLEMS IN THE THEORETICAL ANALYSIS OF THE DATA

Victor J. Slabinski

ABSTRACT

Each INTELSAT IV dual-spin spacecraft carries liquid hydrazine in four conispheric propellant tanks mounted on the spinning rotor section. The destabilizing effect of the liquid on attitude-nutation stability was determined from an extensive series of in-orbit tests. The liquid slosh driving frequency ratio (rotor nutation frequency/rotor spin rate) was varied over the range of 0.58 to 0.70 for the tests by rotating the spacecraft antenna platform at different rates in inertial space. A rotor-mounted accelerometer sensed the spacecraft nutation. The observed time constant for the nutation angle increase or decrease was corrected for the stabilizing contribution of the platform-mounted pendulum dampers to yield the net destabilizing dedamping contribution from the liquid slosh.

The in-orbit tests show two unexpected maxima in the dedamping contribution at driving frequency ratios that vary with the propellant loading. The rotor nutation frequency at the maxima is about one-third of the lowest mode liquid slosh frequency given by ground test data for unspun tanks, and thus does not correspond to a simple resonance of the liquid. Ground tests with spinning systems have produced the same maxima, but the phenomenon is not yet understood.

A preliminary version of this paper appeared in the Proceedings of the CNES-ESA Conference on "Attitude Control of Space Vehicles: Technological and Dynamical Problems Associated with the Presence of Liquids," Toulouse, France, October 10-12, 1977 (ESA SP-129), pp. 87-102. The final version appears in the COMSAT Tech. Rev. 8, 1-40 (Spring 1978).

This paper is based upon work performed at COMSAT-Plaza under the sponsorship of the International Telecommunications Satellite Organization (INTELSAT). Views expressed in this paper are not necessarily those of INTELSAT.

Introduction

Definitions

A dual-spin spacecraft such as INTELSAT IV consists of a spinning rotor section and a normally despun antenna platform, with the two sections connected by a bearing assembly. The bearing axis is the intended spin axis for the spacecraft. This is an unstable axis because, by the common definition of dual-spin spacecraft, it is not the axis of maximum moment of inertia. The bearing axis may exhibit a small motion about the spacecraft's rotational angular momentum vector which is the result of two coning motions, a steady-state motion at a cone half-angle θ_W called the *wobble angle*, and a transient motion called *nutation* whose instantaneous cone half-angle θ_N is the *nutation angle*.

The INTELSAT IV spacecraft carry liquid hydrazine in four partially filled propellant tanks mounted on the rotor section. The liquid motion in response to nutation tends to increase the nutation angle at the rate $k_L\theta_N$, while the platform-mounted pendulum dampers tend to decrease the nutation angle at the rate $k_D\theta_N$. At small nutation angles, the nutation angle is observed to vary exponentially with time t:

$$\theta_N = \theta_{N,0} \exp\left[-\frac{t - t_0}{\tau}\right] \tag{1}$$

where τ is the time constant for nutation angle decay (τ positive) or growth (τ negative). Its inverse can be expressed as the difference of two positive numbers:

$$\frac{1}{\tau} = k_D - k_L \tag{2}$$

where k_D is the *damping contribution* from the platform dampers and k_L is the *dedamping contribution* from liquid slosh on the rotor. The latter contribution will be called "dedamping" for brevity. Spacecraft attitude stability requires $k_L < k_D$ so that τ is positive and any initial nutation damps out. A bound on k_L for all expected operating conditions is thus very important for successful spacecraft design and operation.

The liquid motion in the tanks is commonly referred to as "fuel slosh." This term is not strictly correct here, since hydrazine is a propellant rather than a fuel. Fuel is matter that produces power by combustion, that is, by combination with oxygen, while hydrazine produces its thrust on INTELSAT IV by catalytic decomposition. For this reason, the hydrazine motion will be called *liquid slosh.*

An important determining parameter for liquid slosh effects and hence k_L is the driving frequency ratio, ρ, defined as

$$\rho \equiv \frac{f_d}{\omega_{rz}} \tag{3}$$

where f_d is the liquid driving frequency due to nutation, and ω_{rz} is the rotor spin rate about the bearing axis, both expressed in units of rad/s. The importance of this ratio may be seen by considering that the centrifugal acceleration acting on the liquid in the tanks is $\omega_{rz}^2 R$, where R is some mean liquid distance from the spin axis. The restoring force on the liquid when displaced from equilibrium will be proportional to this acceleration so that the natural frequencies of the liquid are proportional to the square root of this quantity, $\omega_{rz} R^{1/2}$. Since the resonant frequencies are proportional to ω_{rz}, the ratio of driving frequency to liquid resonant frequency is proportional to ρ.

A dual-spin spacecraft offers a distinct advantage for the in-orbit determination of liquid slosh effects because ρ can be varied by merely rotating the platform. The liquid driving frequency during nutation is assumed to be the rotor nutation frequency, $\dot{\lambda}_r$, observed from rotor-fixed axes; hence, the variation of ρ with the platform spin rate ω_{pz} in inertial space is given by

$$\rho = \frac{|\dot{\lambda}_r|}{\omega_{rz}} = \left| \frac{I_{rz}}{I_t} \left[1 - \frac{I_{pz}\omega_{pz}}{H_z} \right]^{-1} - 1 \right| \tag{4}$$

where H_z = bearing axis component of the spacecraft's rotational angular momentum (constant to the first order for small nutation angles)

I_{pz}, I_{rz} = platform and rotor moments of inertia about the bearing axis

I_t = spacecraft moment of inertia about a transverse axis through the mass center.

Since a simple spinner can be considered as the rotor of a dual-spin space-

craft which lacks a platform, setting $I_{pz} = 0$ in equation (4) gives

$$\rho = \left| \frac{I_{rz}}{I_t} - 1 \right| \qquad \text{(simple spinner)} \tag{5}$$

which shows that for a simple spinner ρ is fixed by its mass properties.

Test motivation

Prior to the first INTELSAT IV launch, Hughes Aircraft Co. performed ground tests to predict k_L for the expected spacecraft operating conditions (Reference 1, pp. 75–76). These tests indicated that any nutation would quickly decay, and that k_L was sensitive to ρ variations. However, they were performed for only a few different values of *fill fraction* (the percentage of the propellant tank volume occupied by liquid) and did not indicate two troublesome properties of k_L which were only discovered in 1974 as a result of orbital operation of the INTELSAT IV series of spacecraft. These discoveries raised questions concerning the attitude stability of the INTELSAT IV-A series of communications satellites then under development.

The first was that k_L is a strong function of the driving frequency ratio, ρ. This was discovered during the loss of antenna despin control by the INTELSAT IV F-7 spacecraft on March 21, 1974, when the antenna platform spun up to 25 rpm before recovery; k_L decreased twentyfold during a ρ value change of only 0.03. This discovery, that a small change in ρ can increase or decrease k_L by an order of magnitude, raised the possibility that INTELSAT IV-A, operating at different ρ values, might have k_L values significantly larger than those found previously in INTELSAT IV orbital operation.

This discovery also indicated a need for detailed knowledge of the k_L variation over the range of ρ values possible during an antenna platform spin-up. Such data would indicate whether loss of despin control could result in a rapid growth of the nutation angle to $\sim$90°, the "flat spin" condition from which spacecraft recovery might be difficult. Previous liquid slosh tests on the ground had been restricted to the ρ value corresponding to the despun platform condition.

The second discovery was that k_L appeared to become drastically larger with increasing fill fraction. The first five INTELSAT IV spacecraft launched had a 70-percent fill in transfer orbit after their initial spin-up. The sixth, INTELSAT IV F-8, was launched on November 21, 1974, with a 76-percent fill. The extra propellant was carried as ballast to compensate for an oversized solid propellant apogee motor. Nutation tests in transfer orbit

showed that this extra 6-percent fill doubled k_L. Since this fill fraction region had not been included in the ground tests, this raised a question concerning the magnitude of k_L for the INTELSAT IV-A spacecraft which were to use the same propellant tanks with an initial fill of 82 percent.

To resolve these questions, COMSAT conducted an extensive series of in-orbit nutation tests on the nearly identical spacecraft in the INTELSAT IV series in spring 1975. These tests took place in a 0-g environment and thus avoided the uncertainty inherent in ground testing regarding the correction, if any, which is required for the 1-g field.

Nutation test description

The basic test procedure consists of inducing spacecraft nutation and recording the continuously telemetered output of a nutation accelerometer mounted on the rotor. Figure 1 shows a typical nutation trace for a despun platform. In this case, nutation has been induced by firing an axial thruster for 0.5 s. The sensed acceleration from the nutation oscillates with the rotor nutation frequency, $\dot{\lambda}_r$. This frequency may be determined directly from the time code on the strip chart by noting the time interval for a given number of nutation cycles. Scaling the amplitude at selected points along the nutation trace and fitting equation (1) to the measurements gives the time constant τ for the nutation decay or growth. The computed platform damper contribution k_D is then used in equation (2) to obtain the liquid slosh dedamping k_L.

The in-orbit tests experimentally determined k_L as a function of driving frequency ratio, ρ, and propellant tank fill fraction. The driving frequency ratio was varied by spinning the antenna platform at different rates in inertial space over a range of ± 20 rpm. Obviously, the spacecraft did not carry communications traffic during the tests. Spacecraft with greatly different fill fractions were available, since each satellite of the INTELSAT IV series had been in orbit for a different length of time and had depleted its maneuvering propellant by a different amount. Also, INTELSAT IV F-8 was tested before and after large inclination maneuvers to obtain data at fill fractions of about 66, 61, and 56 percent from the same spacecraft. Finally, to test the initial INTELSAT IV-A fill fraction, the last spacecraft to be launched in the series, INTELSAT IV F-1, was put into orbit loaded with an extra 22 kg of hydrazine propellant to give an initial fill fraction of 82 percent. Most of this extra propellant was expended in transfer orbit to help place this heavily loaded spacecraft into geostationary orbit.

The test data obtained and attempts to understand it are the subjects of this paper. The in-orbit test results prompted an extensive series of

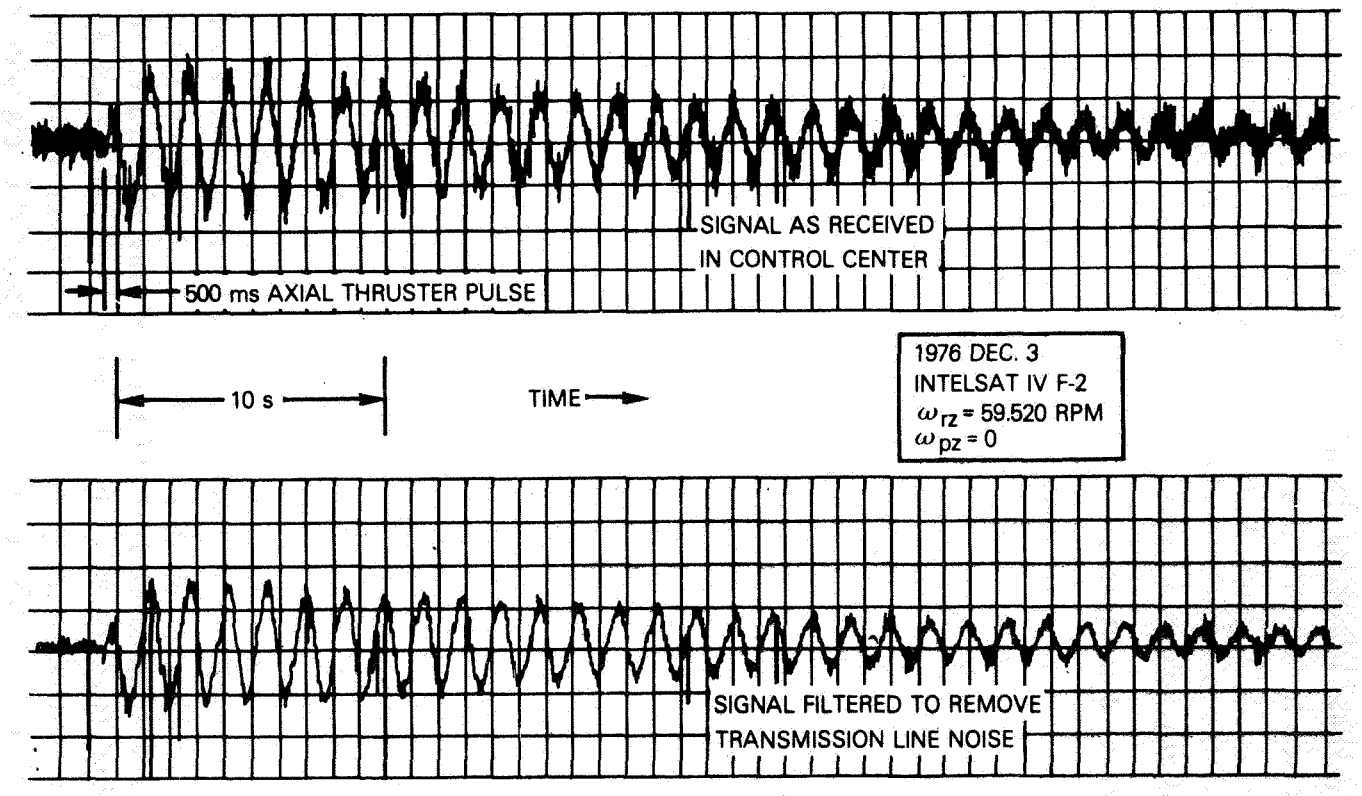

Figure 1. *Nutation Accelerometer Output for a Despun Platform*

liquid slosh ground tests by the spacecraft manufacturer, Hughes Aircraft Co. The large dedamping contributions found in both series of tests resulted in important modifications to the INTELSAT IV-A spacecraft design.

Basic nutation theory

The nutation theory presented herein allows for a cross product of inertia about the platform bearing axis. This cross product introduces additional acceleration frequencies in the rotor propellant tanks. Such additional frequencies due to spacecraft asymmetries may introduce unsuspected slosh effects.

Spacecraft model and platform coordinates

For the present analysis it may be assumed that all damper masses are caged and that the propellant is frozen in its equilibrium position so that each spacecraft section acts as a rigid body. It may also be assumed that the spacecraft is statically balanced so that the mass center of each section lies on the bearing axis. The spacecraft mass center then lies at a point O on the bearing axis which is taken as the origin of a right-handed Cartesian coordinate system $X_pY_pZ_p$ fixed in the platform. The Z_p axis lies along the bearing axis, and the transverse axes X_pY_p are chosen so that there is no platform cross product of inertia about the Y_pZ_p axes. The tensors giving the moments of inertia of the platform and rotor, respectively, are

$$(I_p) = \begin{bmatrix} I_{pt} & 0 & I_{pxz} \\ 0 & I_{pt} & 0 \\ I_{pxz} & 0 & I_{pz} \end{bmatrix}_p \tag{6}$$

$$(I_r) = \begin{bmatrix} I_{rt} & 0 & 0 \\ 0 & I_{rt} & 0 \\ 0 & 0 & I_{rz} \end{bmatrix}_p \tag{7}$$

where the p subscript outside tensor or vector brackets indicates platform-fixed axes. Equation (6) allows for a platform cross product of inertia I_{pxz} since this cross product produces additional acceleration frequencies in the rotor. Equation (7) assumes that the rotor is dynamically balanced so that the bearing axis is a principal axis. Both equations assume equal

moments of inertia I_{pt} and I_{rt} about any transverse axis through O so that the spacecraft moment of inertia about any transverse axis through O is given by

$$I_t = I_{pt} + I_{rt} \tag{8}$$

regardless of the relative orientation between platform and rotor. Another useful quantity is the spacecraft moment of inertia I_z about the bearing axis,

$$I_z = I_{pz} + I_{rz} \tag{9}$$

With respect to the platform-fixed axes, the angular velocities of the platform and rotor sections, respectively, in inertial space are given by

$$\vec{\omega}_p = \begin{bmatrix} \omega_{px} \\ \omega_{py} \\ \omega_{pz} \end{bmatrix}_p \tag{10}$$

$$\vec{\omega}_r = \begin{bmatrix} \omega_{px} \\ \omega_{py} \\ \omega_{rz} \end{bmatrix}_p \tag{11}$$

since the bearing constrains both sections to have the same X_p and Y_p components of angular velocity, ω_{px} and ω_{py}. The $+Z_p$ direction is chosen so that $\omega_{rz} > 0$. The angular momentum, $\vec{H}$, of the spacecraft about its mass center O is then

$$\vec{H} = \begin{bmatrix} H_x \\ H_y \\ H_z \end{bmatrix}_p = (I_p)\,\vec{\omega}_p + (I_r)\,\vec{\omega}_r \tag{12}$$

$$\vec{H} = \begin{bmatrix} I_t\omega_{px} + I_{pxz}\omega_{pz} \\ I_t\omega_{py} \\ I_{pxz}\omega_{px} + I_{pz}\omega_{pz} + I_{rz}\omega_{rz} \end{bmatrix}_p \tag{13}$$

Because the platform-fixed axes rotate with an angular velocity $\vec{\omega}_p$ relative to inertial axes, the time derivative of any vector such as $\vec{H}$ is given by

$$\frac{d\vec{H}}{dt} = \left[\frac{d\vec{H}}{dt}\right]_p + \vec{\omega}_p \times \vec{H} \tag{14}$$

where t is the time, and the brackets around the first term on the right side of the equation indicate a time derivative with respect to rotating axes. In the absence of external torques, $d\vec{H}/dt = 0$ and equation (14) gives

$$\left[\frac{d\vec{H}}{dt}\right]_p = -\vec{\omega}_p \times \vec{H} \tag{15}$$

as the differential equation of motion. In subsequent equations it will be assumed that the despin motor between the platform and rotor sections maintains a constant relative spin rate $\dot{\psi}$ between platform and rotor:

$$\dot{\psi} = \omega_{pz} - \omega_{rz} \tag{16}$$

so that

$$\dot{\omega}_{pz} = \dot{\omega}_{rz} \tag{17}$$

in equation (15), where a dot over a symbol indicates a time derivative.

Steady spin in platform coordinates

The spacecraft model described herein allows steady spin in platform coordinates as given by the following particular solution of equations (13) and (15):

$$\vec{\omega}_{p0} = \begin{bmatrix} \omega_{px0} \\ 0 \\ \omega_{pz0} \end{bmatrix}_p \tag{18}$$

$$\omega_{rz} = \omega_{rz0} = \text{constant} \tag{19}$$

where
$$\omega_{pz0}(I_t\omega_{px0} + I_{pxz}\omega_{pz0}) - \omega_{px0}(I_{pxz}\omega_{px0} + I_{pz}\omega_{pz0} + I_{rz}\omega_{rz0}) = 0 \tag{20}$$

This equation has the solution

$$\frac{\omega_{px0}}{\omega_{rz0}} = \frac{-1 \pm \sqrt{1 + (b\omega_{pz0}/\omega_{rz0})^2}}{b} \tag{21}$$

where b is a dimensionless parameter defined as

$$b = \frac{2I_{pxz}\omega_{rz0}}{I_{rz}\omega_{rz0} + (I_{pz} - I_t)\,\omega_{pz0}} \quad . \tag{22}$$

This paper is concerned with spacecraft for which $|I_{pxz}/I_{rz}| \ll 1$ so that usually $|b| \ll 1$. Then, the ambiguous sign in equation (21) may be taken as positive to obtain a spin vector nearly parallel to the bearing axis. (The negative sign gives the "flat spin" solution.) In this case a binomial expansion of the square root in equation (21) gives

$$\omega_{px0} \simeq \frac{b\omega_{pz0}^2}{2\omega_{rz0}} \tag{23}$$

$$\omega_{px0} = \frac{I_{pxz}\omega_{pz0}^2}{I_{rz}\omega_{rz0} + (I_{pz} - I_t)\,\omega_{pz0}} \quad . \tag{24}$$

Equation (24) shows that, if the platform is spinning ($\omega_{pz0} \neq 0$), a nonzero platform cross product of inertia gives $\omega_{px} \neq 0$ so that steady spin of the spacecraft occurs about a platform-fixed axis that is inclined to the bearing axis. The corresponding rotational angular momentum vector is also fixed in the X_pZ_p plane at an angle θ_W from the bearing axis as obtained from equations (12), (13), (18), and (19):

$$\tan\theta_W = \frac{\sqrt{H_x^2 + H_y^2}}{|H_{z0}|} \tag{25}$$

$$\tan\theta_W = \left|\frac{I_t\omega_{px0} + I_{pxz}\omega_{pz0}}{H_{z0}}\right| \tag{26}$$

where $$H_{z0} = I_{pxz}\omega_{px0} + I_{pz}\omega_{pz0} + I_{rz}\omega_{rz0} \quad . \tag{27}$$

Since $\vec{H}$ is fixed in inertial space, the bearing axis in this motion describes a cone of half-angle θ_W about $\vec{H}$ in inertial space. This is the wobble motion.

Equation (26) may be expressed in a simple form when $|b| \ll 1$ so that equation (24) holds. Equation (24) gives

$$I_{pxz}\omega_{pz0} = \frac{\omega_{px0}}{\omega_{pz0}}\left[I_{rz}\omega_{rz0} + (I_{pz} - I_t)\,\omega_{pz0}\right] \tag{28}$$

which may be used to replace the second term in the numerator of equation (26) to yield

$$\tan\theta_W = \left|\frac{\omega_{px0}}{\omega_{pz0}}\left\{\frac{I_{pz}\omega_{pz0} + I_{rz}\omega_{rz0}}{H_{z0}}\right\}\right| \quad . \tag{29}$$

Equation (27) shows that the expression within the braces is very nearly 1 for a small platform cross product; hence, equations (29) and (24) give

$$\tan\theta_W \simeq \left|\frac{\omega_{px0}}{\omega_{pz0}}\right| \tag{30}$$

$$\tan\theta_W = \left|\frac{I_{pxz}\omega_{pz0}}{I_{rz}\omega_{rz0} + (I_{pz} - I_t)\,\omega_{pz0}}\right| \tag{31}$$

as useful forms for numerical computation. Since H_y is zero here, equations (25) and (30) show that $\vec{\omega}_p$ and $\vec{H}$ are parallel as required by equation (15) for steady spin.

Nutation in platform coordinates

For a dual spin spacecraft, $|I_{pxz}|/I_t$ and $|I_{pxz}|/I_z$ are quantities of the first order of smallness. To sufficient accuracy for this paper, the nutational motion about the steady spin motion is given by

$$\vec{\omega}_p = \begin{bmatrix} \omega_{px0} + \omega_t \cos\lambda_p \\ \omega_t \sin\lambda_p \\ \omega_{pz0} - k_z\omega_t \cos\lambda_p \end{bmatrix}_p \tag{32}$$

$$\omega_{rz} = \omega_{rz0} - k_z\omega_t \cos\lambda_p \tag{33}$$

with

$$k_z \equiv \frac{I_{pxz}}{I_z}\frac{\dot{\lambda}_p + \omega_{pz0}}{\dot{\lambda}_p} \tag{34}$$

and

$$\lambda_p = \lambda_{p0} + \dot{\lambda}_p(t - t_0) \tag{35}$$

where $\dot{\lambda}_p$ is the platform nutation frequency given by

$$\dot{\lambda}_p = \frac{H_{z0}}{I_t} - \omega_{pz0} \quad . \tag{36}$$

λ_{p0} and ω_t are constants of integration, and λ_p essentially gives the azimuth of $\vec{\omega}_p$ about the steady spin solution for platform axes. This solution shows that in the presence of nutation both the platform and rotor spin rates exhibit a small oscillation at the platform nutation frequency when $I_{pxz} \neq 0$, even for the despun platform case ($\omega_{pz0} = 0$).

The accuracy of equations (32) and (33) may be verified by direct substitution into the differential equations of motion, equations (15) and (17). These equations give an exact solution for all ω_t values when $I_{pxz} = 0$; in this case $\omega_{px0} = 0$ from equation (24) and ω_t becomes simply the magnitude of the transverse component of $\vec{\omega}_p$. When $I_{pxz} \neq 0$, the solution is correct for small ω_t values through terms of the first order in $I_t\omega_t/H_{z0}$ provided that $\dot{\lambda}_p$ is not small, more specifically, provided that the inequalities

$$I_t|\dot{\lambda}_p|^j \gg \frac{I_{pxz}^2}{I_z}|\omega_{pz0}|^j \tag{37}$$

hold for $j = 0, 1, 2, 3$. The different j values correspond to different neglected terms in the differential equations. Physically, the platform spin rate $\omega_{pz0} \simeq H_{z0}/I_t$, which gives $\dot{\lambda}_p \simeq 0$, is excluded because the nutational motion assumes a different character which is not of interest for this paper.

For small ω_t values, equations (32), (33), and (13) show that $\vec{H}$ observed from platform axes precesses about its steady spin direction at a nearly constant angle, the nutation angle θ_N:

$$\tan\theta_N \simeq \frac{I_t\omega_t}{H_{z0}} \tag{38}$$

For small angles, θ_N is linearly proportional to ω_t.

Nutation in rotor coordinates

The nutation seen on the rotor is described by using right-handed rotor-fixed Cartesian axes $X_rY_rZ_r$ with the origin at O and the $+Z_r$ axis coin-

cident with the $+ Z_p$ and bearing axes. For these new axes,

$$\vec{\omega}_r = \begin{bmatrix} \omega_{rx} \\ \omega_{ry} \\ \omega_{rz} \end{bmatrix}_r \tag{39}$$

where an r subscript outside vector brackets indicates rotor-fixed axes, and

$$\omega_{rx} = \omega_{px} \cos \psi - \omega_{py} \sin \psi \tag{40}$$

$$\omega_{ry} = \omega_{px} \sin \psi + \omega_{py} \cos \psi \tag{41}$$

where ψ gives the angle about the bearing axis between the $+X_r$ and $+X_p$ directions. Equations (32), (33), (35), (36), and (17) then give

$$\vec{\omega}_r = \begin{bmatrix} \omega_{px0} \cos \psi + \omega_t \cos \lambda_r \\ \omega_{px0} \sin \psi + \omega_t \sin \lambda_r \\ \omega_{rz0} - k_z \omega_t \cos \lambda_p \end{bmatrix}_r \tag{42}$$

where $$\lambda_r = \lambda_p + \psi = \lambda_{r0} + \dot{\lambda}_r (t - t_0) \quad . \tag{43}$$

In equation (43), $\dot{\lambda}_r$ is the rotor nutation frequency given by

$$\dot{\lambda}_r = \dot{\lambda}_p + \dot{\psi} \tag{44}$$

$$\dot{\lambda}_r = \dot{\lambda}_I - \omega_{rz0} \tag{45}$$

where

$$\dot{\lambda}_I = \frac{H_{z0}}{I_t} \quad . \tag{46}$$

$\dot{\lambda}_I$ is the inertial nutation rate at small nutation angles, the rate at which the bearing axis precesses about $\vec{H}$ in inertial space. Note that terms with three different frequencies are present in the rotor angular velocity.

Equation (45) shows that $\dot{\lambda}_r$ may be arbitrarily varied in the in-orbit

tests. Since $I_{pxz} \sim 0$, changing the platform spin rate varies ω_{rz0} but not $\dot{\lambda}_I$ because H_z stays constant. From equation (27), in the absence of thruster pulses,

$$H_{z0} = I_{pz}\omega_{pz0} + I_{rz}\omega_{rz0} = I_{rz}\omega_{rzd} = \text{constant} \tag{47}$$

where ω_{rzd} is the rotor spin rate with the platform despun. Equation (45) may be written as

$$\dot{\lambda}_r = \frac{I_{rz}}{I_t}\,\omega_{rzd} - \omega_{rz0} \quad . \tag{48}$$

Eliminating ω_{rz0} from equations (45) and (47) yields equation (4) for the variation of ρ as a function of ω_{pz0}. An alternate form giving ρ as a function of $\dot{\psi}$ is obtained by eliminating ω_{pz0} and ω_{rz0} from equations (16), (47), and (48):

$$\rho = \left| \frac{I_z}{I_t}\left[1 - \frac{I_{pz}\dot{\psi}}{I_{rz}\omega_{rzd}}\right]^{-1} - 1 \right| \quad . \tag{49}$$

Rotor accelerations and accelerometer

The acceleration $\vec{a}$ about the spacecraft mass center O of a point P fixed in the rotor is obtained as follows. The X_r axis may be chosen so that the position vector for P is given by

$$\vec{r} = \begin{bmatrix} R_p \\ 0 \\ z_p \end{bmatrix}_r \tag{50}$$

This point has a velocity $\vec{\omega}_r \times \vec{r}$ about O; hence, for rotating rotor axes,

$$\vec{a} = \left[\frac{d}{dt}(\vec{\omega}_r \times \vec{r})\right]_r + \vec{\omega}_r \times (\vec{\omega}_r \times \vec{r}) \tag{51}$$

$$\vec{a} = \left[\frac{d\vec{\omega}_r}{dt}\right]_r \times \vec{r} + \vec{\omega}_r(\vec{\omega}_r \cdot \vec{r}) - \vec{r}\omega_r^2 \quad . \tag{52}$$

Keeping terms to first order in ω_{px0} and ω_t in using equation (42) to eliminate $\vec{\omega}_r$ gives

$$\vec{a} = \begin{Bmatrix} R_p\,[-\omega_{rz0}^2 + 2k_z\omega_t\omega_{rz0}\cos\lambda_p] \\ \quad + z_p\,[\omega_{px0}\omega_{pz0}\cos\psi + \omega_t(\dot{\lambda}_r + \omega_{rz0})\cos\lambda_r] \\ R_p[k_z\omega_t\dot{\lambda}_p\sin\lambda_p] \\ \quad + z_p\,[\omega_{px0}\omega_{pz0}\sin\psi + \omega_t(\dot{\lambda}_r + \omega_{rz0})\sin\lambda_r] \\ R_p\,[\omega_{px0}(2\omega_{rz0} - \omega_{pz0})\cos\psi \\ \quad + \omega_t(-\dot{\lambda}_r + \omega_{rz0})\cos\lambda_r] \end{Bmatrix} \tag{53}$$

The large constant term $-R_p\omega_{rz0}^2$ in the X_r axis component gives the centripetal acceleration due to rotor spin.

Equation (53) makes it possible to interpret the output of an accelerometer located at P. There are two accelerometers mounted on the rotor at $R_p = 0.99\ m$ with their sensitive axis parallel to the bearing (Z_r) axis. Filtering their output to pass only frequencies between 0.03 and 35 Hz eliminates any contribution from the large X_r axis constant term that might be sensed due to accelerometer misalignment. The filtered output is transmitted by FM real-time telemetry to the ground where it is detected and displayed versus time on a strip chart recorder. The filter readily passes both Z_r axis terms for INTELSAT IV at its typical 50-rpm rotor spin rate: the wobble term with frequency $\dot{\psi} \sim -5$ rad/s and amplitude

$$A_W = R_p\omega_{px0}(2\omega_{rz0} - \omega_{pz0}) \tag{54}$$

$$A_W \simeq \frac{R_p I_{pxz}(2\omega_{rz0} - \omega_{pz0})\,\omega_{pz0}^2}{I_{rz}\omega_{rz0} + (I_{pz} - I_t)\,\omega_{pz0}} \tag{55}$$

from equations (53) and (24), and the nutation term with frequency $\dot{\lambda}_r \sim -4$ rad/s and amplitude proportional to ω_t, so that it is a measure of the nutation angle. For small platform spin rates, equation (55) gives the approximation

$$A_W \simeq 2R_p\frac{I_{pxz}}{I_{rz}}\,\omega_{pz0}^2 \tag{56}$$

which shows that the wobble term amplitude depends on the ratio I_{pxz}/I_{rz}.

Both the wobble and the nutation terms can appear in the nutation trace and thereby produce a beat phenomenon when the platform spins as shown in Figure 2 for INTELSAT IV-A, for which $I_{pxz}/I_{rz} = 0.06$. This

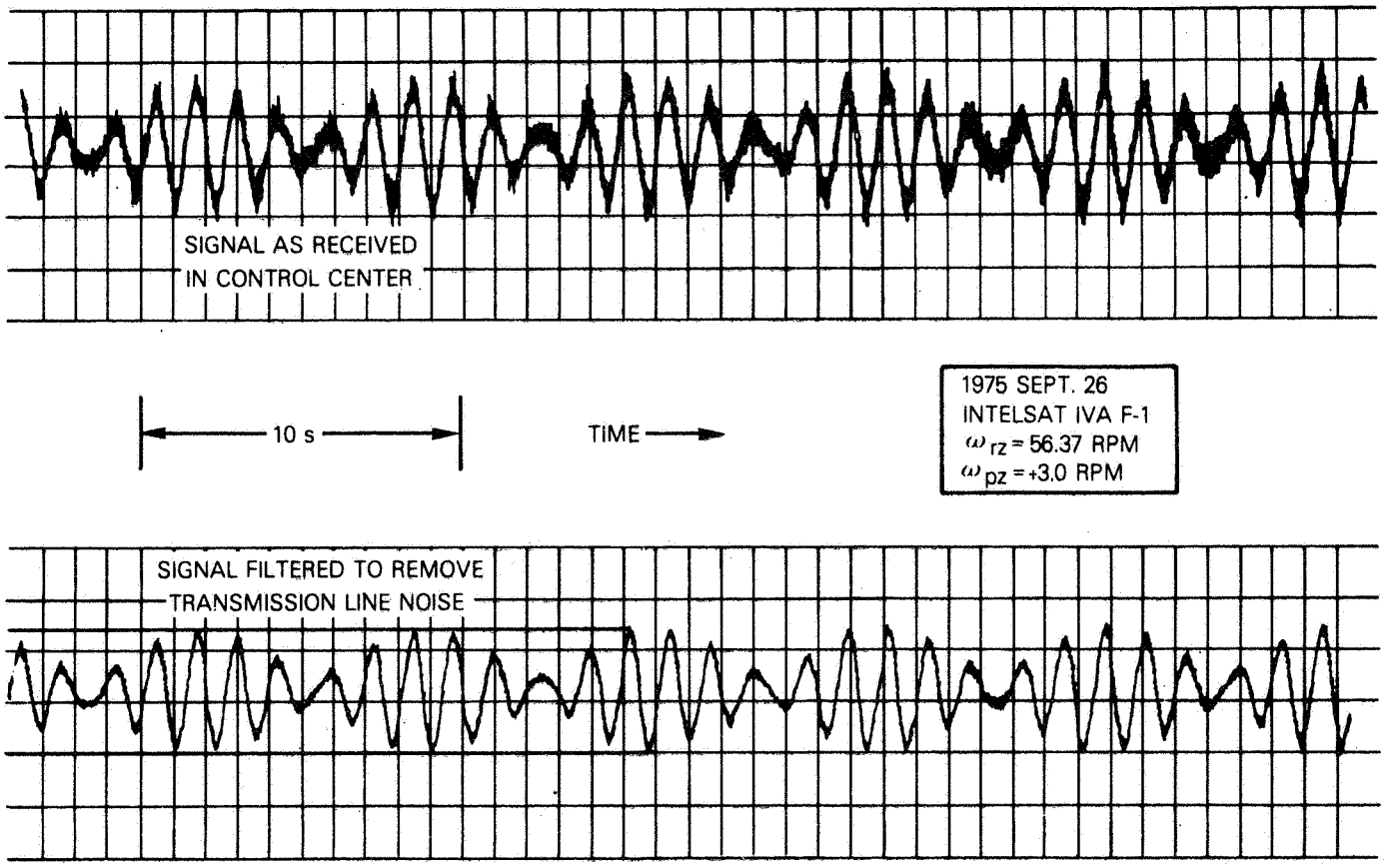

Figure 2. *Nutation Accelerometer Output for a Spinning Platform with a Large Inertial Cross Product*

moment of inertia ratio is large because of the INTELSAT IV-A antenna mast design. The resulting wobble term completely dominates the nutation trace at high platform spin rates and complicates the hand reduction of the nutation strip charts to yield nutation time constants. It is also possible that the liquid excitation by a large wobble term results in a significant contribution to the observed dedamping. INTELSAT IV does not have these problems because its antenna platform was dynamically balanced about the bearing axis to give a small I_{pxz} value. Its observed wobble motion gives $|I_{pxz}| \sim 0.13\ kg \cdot m^2$ so that $I_{pxz}/I_{rz} \sim 0.0006$ for this spacecraft. Thus, INTELSAT IV is ideally suited for spinning platform slosh tests. Its wobble term is detectable for $|\omega_{pz0}| > 8$ rpm, but becomes troublesome only for $\omega_{pz0} \sim 18$ rpm near the $\dot{\lambda}_p \sim 0$ platform resonance.

Note that some terms in $\vec{a}$ with frequency $\dot{\lambda}_p \sim 2$ rad/s are not detected by the rotor accelerometer because they do not appear for the Z_r axis. This observation indicates that all the rotor acceleration frequencies which might produce liquid slosh cannot be determined by merely performing a spectrum analysis of the telemetry record.

If P is a point in the propellant tank liquid, the Y_r and Z_r axis components of $\vec{a}$ give the driving accelerations parallel to the free liquid surface which produce liquid slosh. The terms proportional to ω_t are responsible for the dedamping, since their effect on the liquid increases with the nutation angle. Such terms here have two different frequencies, $\dot{\lambda}_r$ and $\dot{\lambda}_p$, which are not harmonically related. The $\dot{\lambda}_p$ terms are *not* due to nonlinear effects, but arise from a theory linear in ω_t. The $\dot{\lambda}_r$ terms have the largest amplitude by a factor of 100; hence, this paper adopts the usual assumption that these terms give the only significant accelerations producing liquid slosh. The $\dot{\lambda}_p$ terms should not be completely dismissed, however. Although the $\dot{\lambda}_p$ term in the Y_r component has the small factor k_z, the liquid response at this frequency could be very large if $|\dot{\lambda}_p|$ equalled a natural frequency of the liquid. Note that this term persists even for a despun platform.

Theoreticians should develop the complete theory of such small acceleration terms due to vehicle inertia asymmetries and mass center misalignments because of the possibility of frequency coincidence with liquid resonances. It is possible that such a frequency coincidence with a well-understood liquid resonance might explain the anomalous resonances observed in orbit. Similar small acceleration terms should also occur for spinning test fixtures on the ground due to interactions with the earth's gravitational field. The amplitudes of such terms do not necessarily become zero because of a rapid vehicle spin rate.

Nutation test details

Nutation test procedure

The INTELSAT IV pendulum dampers are mounted in an open frame structure on the antenna platform. As a result, their temperature undergoes a large daily variation over a range of 100°C due to changes in shadowing and the direction of the incident sunlight as the earth-pointing antenna platform rotates at 1 rev/day in inertial space. This temperature variation causes a 40-percent change in the eddy-current damping force. To eliminate this variation from an extensive series of nutation tests extending over many hours, the platform was spun in sunlight in a "rotisserie mode" at 1 rpm for 6 hours before the tests to establish an equilibrium temperature.

For each test, the antenna despin control electronics were operated in the rate memory hold mode (Reference 2, pp. 295–299) and commanded to the proper relative spin rate $\dot{\psi}$ computed from equation (49) to give the desired ρ value. Spacecraft telemetry sent through an omnidirectional antenna indicated when the desired platform spin rate had been established. This spin rate can also be measured directly by recording the signal level of a carrier sent through a global beam antenna on the platform; the signal strength rises from zero once each platform spin period as the global beam illuminates the earth. With the spin rate established, accelerometer data were usually obtained over at least one nutation time constant. Only for tests with $\tau > 600$ s was this not always done.

For some unstable platform spin rates, the small nutation already present from starting transients would quickly increase to measurable levels. For other spin rates, measurable nutation was already present from a previous test. An axial thruster was fired to induce nutation only when necessary to avoid violating thermal constraints on thruster restarts at short time intervals. The tests were restricted to nutation angles less than 1°. To reduce the nutation angle following tests that gave unstable nutation, the platform was returned to the rotisserie mode or to some other platform spin rate that gave stable nutation rather than to the despun condition, in order to maintain the damper equilibrium temperature.

For the most accurate presentation of the data, the value of $\dot{\lambda}_r$ used to compute the ρ value actually occurring in each test should be measured on the nutation strip chart recording. For most of the tests, $\dot{\lambda}_r$ was computed from equation (48) simply because the rotor spin rate is readily obtained by telemetry from the rotor-mounted sun and earth sensors. Equation (48) gives a useful check on the spacecraft mass properties com-

puted from prelaunch measurements, but it strictly holds only for a rigid spacecraft. Liquid slosh in response to nutation may result in measurable differences from the values of equation (48). These differences could provide clues to the nature of the anomalous liquid resonances observed in the tests.

Reference 2 describes the INTELSAT IV spacecraft in great detail. Table 1

TABLE 1. MASS PROPERTIES FOR INTELSAT IV F-8

	Transfer Orbit	Synchronous Orbit	
		Start of Life	End of Life
Spacecraft Mass (kg)	1,404	753	608
Hydrazine Mass (kg)	144	142	0
Fill Fraction, f	0.758	0.747	0
Tank Center Location z_T Above Spacecraft Mass Center O (m)	+0.24	−0.24	−0.30
Moments of Inertia (kg m^2)			
I_{pz}	93	93	93
I_{rz}	321	255	201
I_t	1,131	702	663

lists the mass properties of a typical INTELSAT IV spacecraft based on ground measurements; adequate moment of inertia values for other synchronous orbit hydrazine loadings may be found by linear interpolation in the table. The following two subsections provide those details on the platform nutation dampers and propellant tanks necessary for a detailed understanding of the in-orbit tests.

Platform nutation dampers

Neer [1] adequately describes the two platform-mounted pendulum nutation dampers on INTELSAT IV and gives typical parameter values. The damping contribution from the ith damper is given by

$$k_{D,i} = \frac{m_i z_{Di}^2}{I_t} \frac{\dot{\lambda}_I^3(\zeta_i \omega_{ni} \dot{\lambda}_p)}{(\omega_{ni}^2 - \omega_{pz}^2 - \dot{\lambda}_p^2)^2 + 4(\zeta_i \omega_{ni} \dot{\lambda}_p)^2} \tag{57}$$

where m_i = mass of the ith damper pendulum

z_{Di} = distance along the spacecraft bearing axis from the spacecraft mass center to the ith pendulum mass

ω_{ni} = natural frequency of the ith pendulum

ζ_i = damping factor expressed as fraction of critical damping.

Haines and Leondes [3] derive this result using an energy sink model, which is an adequate approximation for this paper. The form of the equation presented here avoids singularities at $\dot{\lambda}_p = 0$. Superposition is assumed to hold so that

$$k_D = k_{D,1} + k_{D,2} \quad . \tag{58}$$

Equations (57) and (58) were evaluated for each nutation test based on preflight ground measurements of the damper parameters. Then the liquid dedamping could be evaluated from the observed nutation time constant τ using equation (2) rewritten in the form

$$k_L = k_D - \frac{1}{\tau} \quad . \tag{59}$$

In some tests, the dedamping contribution is negligible compared to the damping contribution so that the right side of equation (59) involves the difference of two nearly equal numbers. The computed k_L values are very uncertain in such cases; therefore, such values have not been included in this paper.

The pendulum dampers swing in a plane parallel to the bearing axis but are not mounted directly on the bearing axis. At platform spin rates with absolute values above $\sim$10 rpm, centrifugal forces peg the dampers against their stops, which prevents them from swinging. The most accurate dedamping values are determined with the dampers pegged because their damping contribution is then zero and $k_L = -1/\tau$ with no error due to uncertain damper parameters. The pegged dampers contribute an almost negligible 0.2 $kg \cdot m^2$ to I_{pxz}.

Conispheric propellant tanks and fill fraction

Four conispheric tanks are mounted on the rotor at intervals of 90° about the bearing axis. Two such tanks are shown in cross section in Figure 3. The tank interior consists of a spherical section with an internal

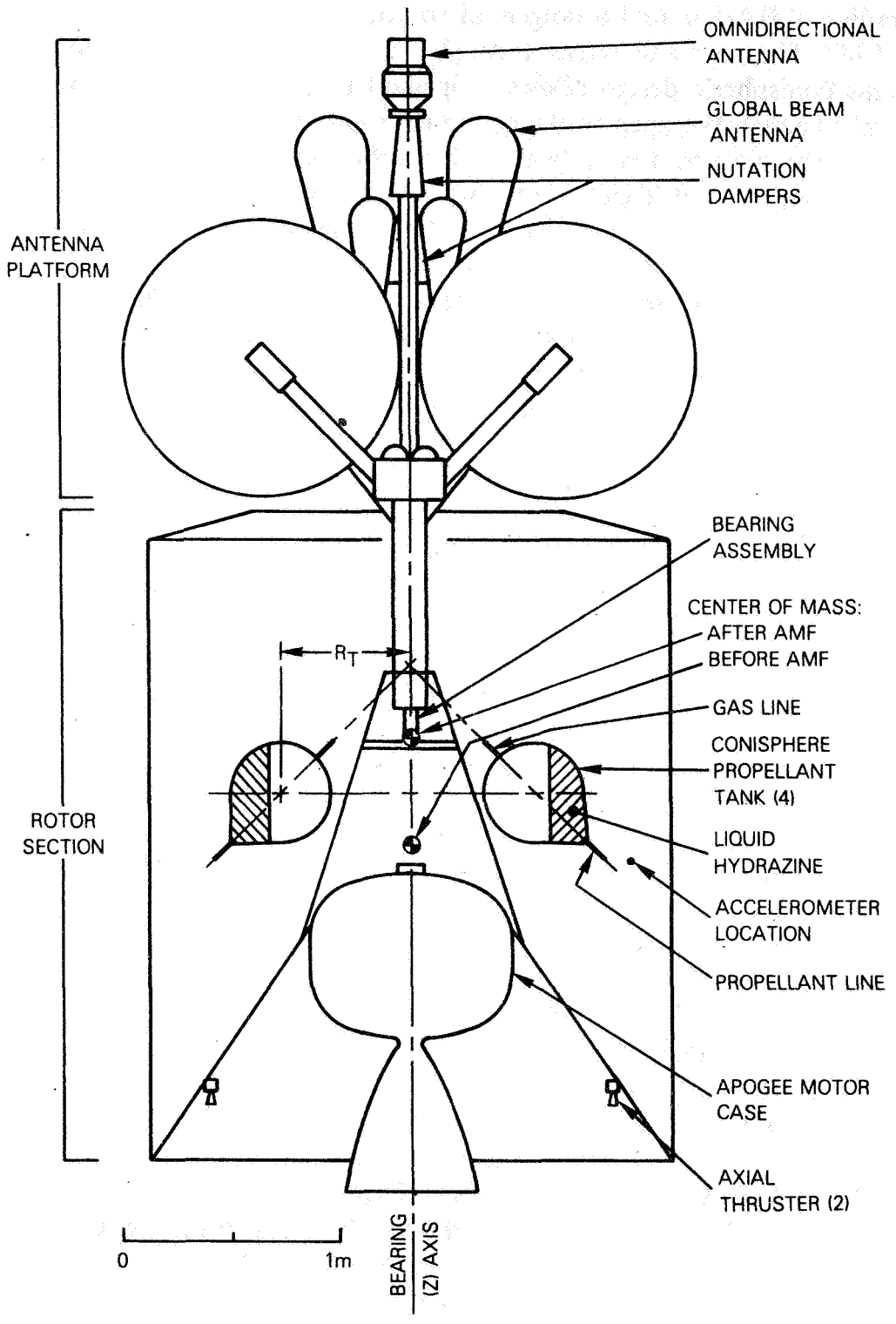

Figure 3. *INTELSAT IV Spacecraft with Cutaway View of Rotor Section*

radius of 0.221 *m* and a tangential conical section with a full cone angle of 85°. The cone axis passes through the bearing axis at an angle of 45°. This conispheric design allows propellant to drain completely from the tank through the apex of the cone under two conditions: on the ground when the spacecraft is vertical, and in orbit during thruster firings under the action of centrifugal forces and nitrogen gas pressurant in the tank. In theoretical discussions for fill fractions greater than 40 percent, the tanks are often assumed to be spherical since the conical section is then nearly full and the free liquid surface lies almost entirely within the spherical section. The cone volume outside a sphere inscribed in the tank is only 3.7 percent of the tank volume.

There are two independent propulsion subsystems; each pair of diametrically opposite tanks is connected to the same subsystem by two lines. A gas pressure equalization line connects at the point on the spherical wall directly opposite the cone apex, and a common propellant line connects at the cone apex so that the two tanks may drain evenly during use and maintain rotor balance. There is no oscillating transfer of liquid between tanks in response to nutation because of the high flow resistance in the connecting propellant line. This resistance is due to the length (3.25 m) and small inside diameter (5.3 mm) of the line. A high resistance is confirmed by the very long (18-min) time constant observed for the in-orbit liquid redistribution between tanks after an initial imbalance [4]. It will be assumed that the two tanks in a subsystem have identical fill fractions.

The center of each spherical section lies at a distance $R_T = 0.578$ m from the bearing axis, and at a bearing axis position $z_T = +0.24$ m above the spacecraft mass center O while in transfer orbit. The expulsion of 650 kg of solid propellant during apogee motor firing (AMF) shifts O toward the antenna platform so that $z_T = -0.24$ m after AMF. Since the tanks are nearly the same distance from O before and after AMF, it should be possible to combine dedamping values determined before and after. This is desirable because of the different ρ values obtainable before and after AMF; ρ due to nutation with the platform despun changes from 0.72 to 0.64.

The following considerations enter into the computation of the tank fill fraction. Hughes Aircraft Co. reports that each INTELSAT IV tank has an internal volume of 0.04689 m^3 on the average with a standard deviation of 0.14 percent. Multiplying this volume by 1.008×10^3 kg/m^3, the density of hydrazine at the tank operating temperature of 20°C, gives 47.26 kg for the hydrazine capacity of an unpressurized tank. The initial nitrogen gas pressure of 1.7 MN/m^2 increases the tank volume by 0.10 percent because of the thin wall construction. This volume increase is

reduced as the gas pressure decreases to 0.7 MN/m² with the depletion of propellant. The volume change should be included in the computation of the fill fraction for comparison of in-orbit tests with ground test data because the ground tests are often made with unpressurized tanks. The fill fraction, f, is computed by correcting the propellant mass, m_p (in kg), in the propulsion system for the propellant in the connecting lines and the spin-up thruster propellant reservoir (about 0.31 kg for each subsystem) to find the mass actually in the tanks; this figure is then divided by the total mass that the two tanks can hold at the existing pressure:

$$f = \frac{m_p - 0.31 \text{ kg}}{2(47.26 \text{ kg})\,[1 + (0.0006 \text{ m}^2/\text{MN})\,p]} \tag{60}$$

where the tank pressure, p (in MN/m²), is given by spacecraft telemetry. This formula has been used to compute all the in-orbit fill fractions quoted in this paper.

The propellant mass on board a spacecraft is somewhat uncertain because it is based on bookkeeping records of maneuvers and a predicted value of propellant flow when a thruster valve is opened. The accuracy of this propellant accounting was recently checked at COMSAT for some INTELSAT III satellites built by TRW, Inc. In May of 1977, the hydrazine was used to exhaustion in propelling these satellites into orbits high above synchronous altitude where they were abandoned. The end of spin speed changes and an accompanying more rapid drop in tank pressure indicated the point of exhaustion. Table 2 lists the hydrazine remaining in each system at this point according to COMSAT's accounting.

TABLE 2. INTELSAT III HYDRAZINE USE ACCOUNTING ERRORS

Parameter	INTELSAT III F-2 Propellant System		INTELSAT III F-6 Propellant System	
	1	2	1	2
Hydrazine at Launch (kg)	10.91	10.91	10.30	10.30
Hydrazine Left According to Accounting at Exhaustion (kg)	0.50	1.13	0.18	0.54
Accounting Underestimate of Propellant Use (%)	4.6	10.4	1.8	5.3
mean (%)	5.5			
standard deviation (%)	±3.1			

Table 2 shows that the accounting underestimated the propellant use by an average of 5.5 percent. If a similar error occurs for INTELSAT IV, the fill fractions listed in this paper for the most depleted tanks will be in error by 1 percent.

Nutation test results and interpretation

Data scaling

It is first necessary to consider whether any scaling should be applied to the observed dedamping values to make the data independent of arbitrary test parameters such as the rotor spin rate. For this discussion, a particular model for liquid slosh is assumed, not because this model accurately reflects reality, but only because it provides a simple illustration of scaling problems. Specifically, it is assumed that liquid slosh produces its destabilizing effect by the back and forth pendulum motion of the liquid mass in response to the nutation. Iorillo [5] models the liquid by an analogous mass-spring-dashpot damper mounted on the rotor at the tank center. This damper will be called the *Iorillo slosh model.* Iorillo shows that the dedamping from longitudinal oscillation (oscillation parallel to the bearing axis) is then given by

$$k_{Lz} = \frac{-R_T^2}{2I_t} \frac{(\dot{\lambda}_r + \omega_{rz})(\dot{\lambda}_r - \omega_{rz})^2 \dot{\lambda}_r c_d}{(\dot{\lambda}_r^2 - \omega_d^2)^2 + (\dot{\lambda}_r c_d / m_d)^2} \tag{61}$$

where c_d is the damping constant (the resistive force per unit velocity), m_d is the mass, and ω_d is the natural frequency of the damper. A similar expression holds for transverse oscillation, with R_T^2 replaced by z_T^2. Because $\dot{\lambda}_r$ is generally negative for a dual spin spacecraft, the driving frequency ratio is given by

$$\rho = \frac{-\lambda_r}{\omega_{rz}} \tag{62}$$

and

$$k_{Lz} = \frac{R_T^2}{2I_t} \frac{(1 - \rho)(1 + \rho)^2 \rho c_d}{(\rho^2 - \rho_{res}^2)^2 + \{\rho c_d / (m_d \omega_{rz})\}^2} \tag{63}$$

where

$$\rho_{res} = \frac{\omega_d}{\omega_{rz}} \tag{64}$$

gives the resonant frequency ratio. For the liquid case, since ω_d is propor-

tional to ω_{rz} as previously explained, ρ_{res} is independent of ω_{rz}.

The following special cases give the two extremes for spin rate scaling. For small damping constants, the expression within braces in the denominator is much smaller than ρ_{res}^2. Then, for frequency ratios far below and far above resonance,

$$k_{Lz} \simeq \frac{R_T^2}{2I_t} \frac{(1-\rho)(1+\rho)^2 \rho c_d}{\rho_{res}^4} \qquad (\rho \ll \rho_{res}) \tag{65}$$

$$k_{Lz} \simeq \frac{R_T^2}{2I_t} \frac{(1-\rho)(1+\rho)^2 \rho c_d}{\rho^4} \qquad (\rho \gg \rho_{res}) \tag{66}$$

and the dedamping is independent of rotor spin rate. This is one scaling extreme. At the damper resonance,

$$k_{Lz} = \frac{R_T^2}{2I_t} \frac{(1-\rho_{res})(1+\rho_{res})^2 m_d^2 \omega_{rz}^2}{\rho_{res} c_d} \qquad (\rho = \rho_{res}) \tag{67}$$

and the dedamping varies as the square of the rotor spin rate. This is the opposite scaling extreme.

These three cases indicate a scaling caveat: the dedamping value measured at a single rotor spin rate cannot be scaled to a different spin rate without some detailed knowledge of the dedamper mechanism such as the relation between the frequency ratio used in the test and resonance. Therefore, scaling will not be applied to the observed dedamping values with the exception of the following application. Equation (63) indicates that the dedamping value k_L measured for a spacecraft varies inversely with its transverse moment of inertia, I_t, so that the dedamping k_L' for a spacecraft with a different transverse inertia I_t' but identical tank geometry relative to the mass center is given by

$$k_L' = \frac{I_t}{I_t'} k_L \quad . \tag{68}$$

This scaling is used to combine transfer orbit data with data taken after AMF.

An important scaling application is the spin rate scaling of ground measurements using spinning test fixtures to orbiting satellites. These

ground tests usually involve very high spin rates to obtain a high Froude number, F_R (the ratio of centrifugal acceleration to gravitational acceleration), at the tank in order to minimize gravitational effects, while the in-orbit satellite has a much lower spin rate. However, the following difficulty arises when scaling isolated dedamping values from ground tests using full scale tanks. For isolated test points, the relation between the driving frequency ratio used and the liquid resonances is not known; hence, the scaling caveat just given warns that a simple scaling is not possible. In addition, an upper bound on the in-orbit dedamping may be obtained by using the scaling extreme from the Iorillo slosh model that gives the highest (most pessimistic) dedamping value. For scaling to lower spin rates, an upper bound is thus obtained by assuming that dedamping is independent of spin rate.

Cautions on the time constant group

The time constant group is discussed here since this quantity is sometimes misapplied in spin rate scaling. From a dimensional analysis, Neer and Salvatore, in Chapter 4 of Reference 6, propose the *dimensionless* time constant group τ_{cg} as a convenient parameter for correlating ground and in-orbit dedamping measurements. They give

$$\tau_{cg} = \frac{n\mu d_T^5 \omega_{rz} \tau_{DD}}{I_t} \tag{69}$$

$$\tau_{cg} = \text{function } (R_e, F_R, f, S, \rho, d_T/R_T, z_T/R_T) \tag{70}$$

where n = number of tanks

μ = mass density of the liquid

d_T = a characteristic tank dimension such as the sphere diameter for conispheric tanks

τ_{DD} = dedamping "time constant"

F_R = Froude number at the tank

$\equiv$ centrifugal acceleration of tanks/gravitational acceleration (an infinite ratio in a 0-g field)

S = tank shape factor

R_T = distance of the tank (sphere) center from the bearing axis

z_T = tank height above spacecraft mass center

$$\tau_{DD} \equiv \frac{1}{k_L} \tag{71}$$

with the Reynolds number R_e defined as

$$R_e = \frac{\rho \omega_{rz} \mu d_T^2}{\eta} \tag{72}$$

where η is the liquid viscosity.

The functional relation in equation (70) is to be discovered empirically by experiment. This functional relation is useful only if the dimensionless parameters in the argument list can be varied individually. However, for the in-orbit dedamping measurements described herein, at least two of the parameters are always varied simultaneously; spinning the antenna platform at different inertial spin rates varies not only ρ but also R_e through the accompanying rotor spin rate change, as shown by equation (72). Therefore, the present paper does not use the time constant group.

For applications, equations (69) and (71) yield

$$k_L = \frac{n \mu d_T^5 \omega_{rz}}{I_t \tau_{cg}} \tag{73}$$

This equation must always be applied cautiously because τ_{cg} can be a function of the other parameters on the right side of the equation. For example, equation (73) gives no definite theoretical relation between k_L and ω_{rz} since equations (70) and (72) indicate that τ_{cg} is a possible function of ω_{rz} through the Reynolds number. From ground test data, Neer and Salvatore conclude in Chapter 7 of Reference 6 that τ_{cg} is independent of ω_{rz} at a resonance (k_L maximum); then k_L varies *linearly* with the rotor spin rate. Equation (67) from the Iorillo slosh model predicts a different result in this case, that k_L varies as *the square* of the rotor spin rate. If the Neer and Salvatore linear dependence could be verified by in-orbit tests, it could provide a valuable clue to the nature of the observed dedamping resonances.

Observed liquid resonances

Figures 4–8 show the observed dedamping values plotted versus the driving frequency ratio for various fill fractions. Figure 8, which com-

pares three different fill fractions, clearly shows that a change of a few percent in the fill fraction can result in a drastic change in the dedamping for a given ρ value. Note especially the increase in dedamping with increasing fill fraction at $\rho = 0.72$, the ratio for a despun platform while in transfer orbit. Each figure lists the dates for the nutation tests, the satellite used, and the satellite I_t value at the time of the tests for data scaling applications using equation (68). Figure 8 includes transfer orbit data scaled to the value $I_t' = 700\ \text{kg}\cdot\text{m}^2$ so that they may be readily compared with the rest of the data taken after AMF. The fill fractions for both propellant systems are always given since they may be very unequal.

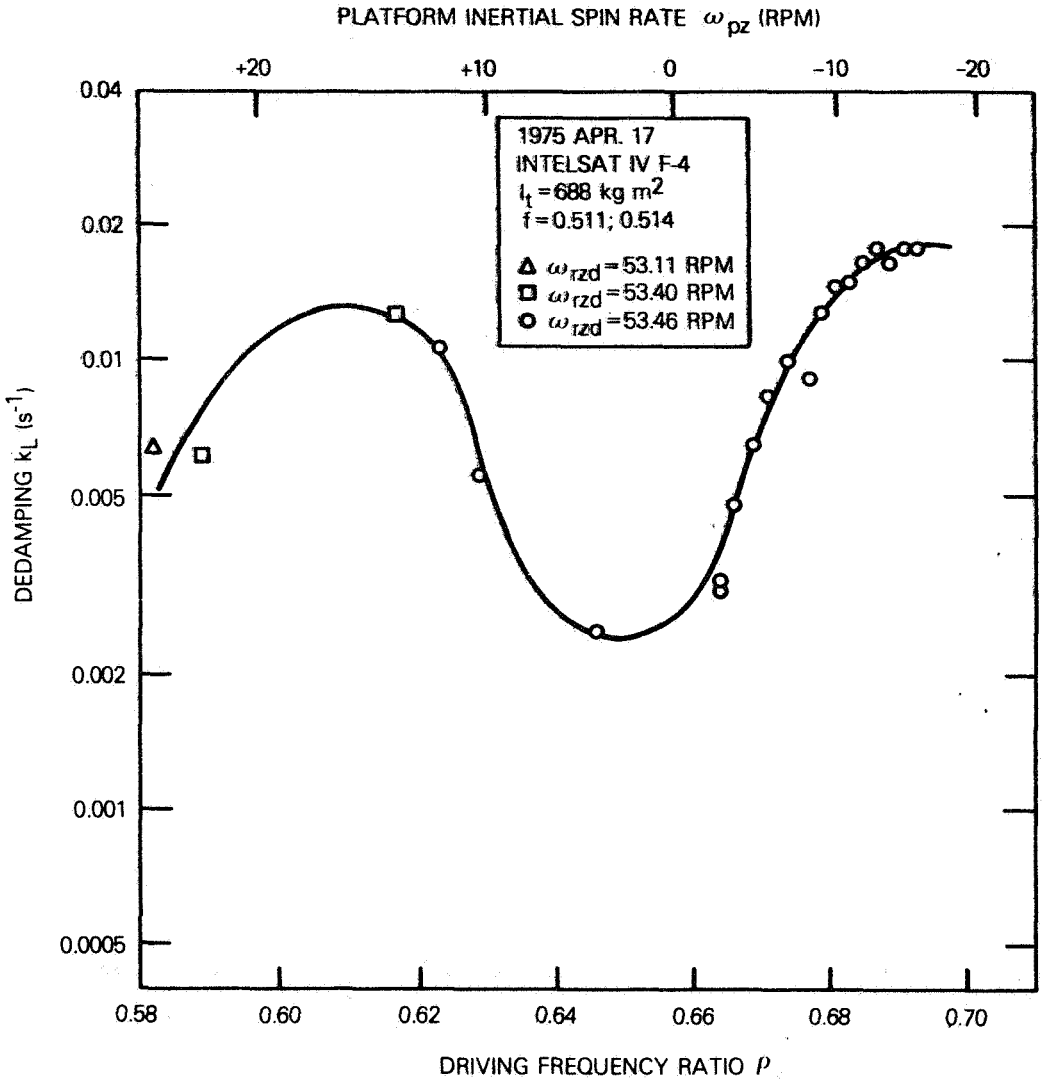

Figure 4. *Tank Liquid Dedamping Contribution for a 51-Percent Fill Fraction*

The data show distinct dedamping maxima which are interpreted as liquid resonances. These are called the *anomalous resonances* since their origin is not known. Two maxima are evident in some of the data: Figure 4 definitely shows two peaks, while Figure 5 shows one peak and part of a second. Figure 9 shows that the frequency ratio ρ_{res} at a maximum moves to higher values with increasing fill fraction, indicating that the anomalous resonances are actually due to the presence of liquid hydrazine on the rotor. Parallel straight lines have been drawn on the graph to indicate the trend of the data.

Thruster firings during some test series changed the spacecraft rota-

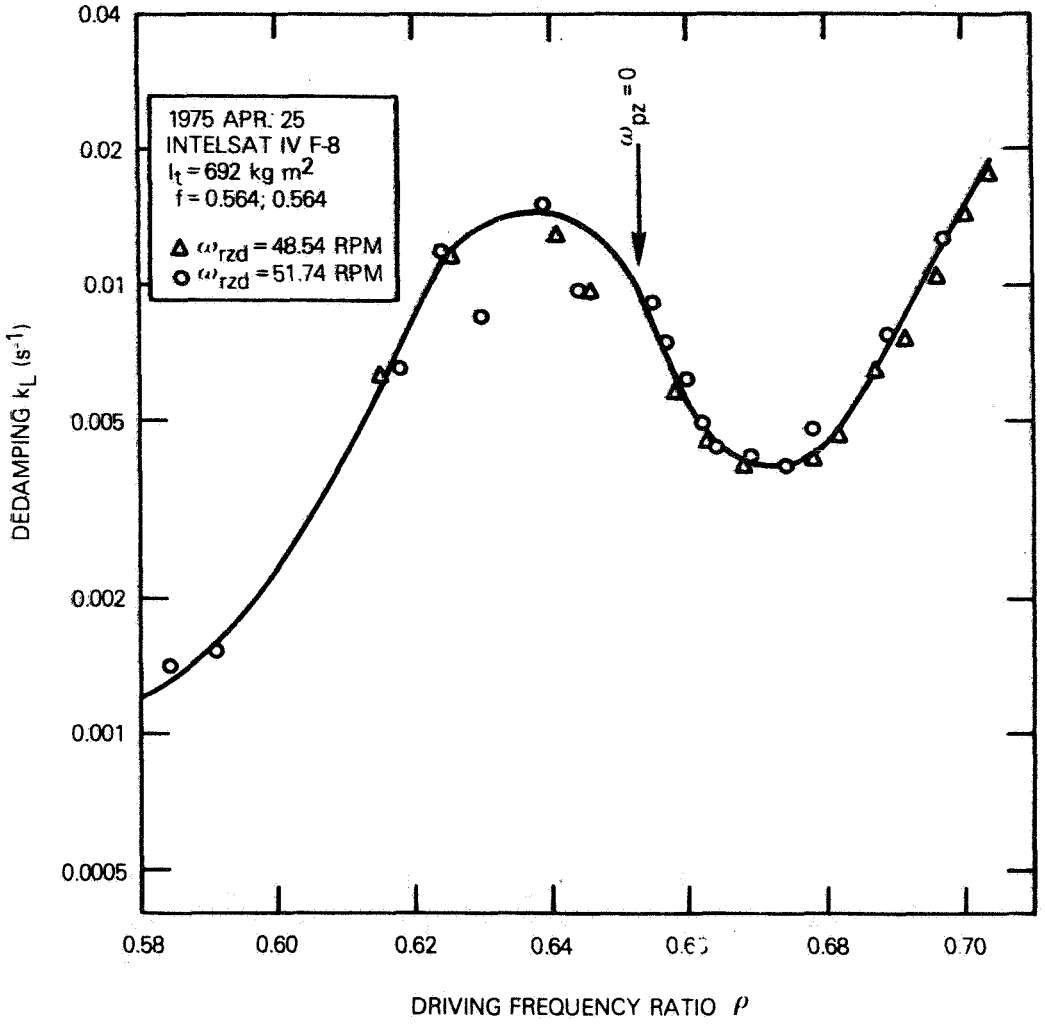

Figure 5. *Tank Liquid Dedamping Contribution for a 56-Percent Fill Fraction*

tional angular momentum so that different data sets for a given fill fraction may correspond to a significantly different rotor spin rate ω_{rzd} with the platform despun. Such data sets are distinguished by different plotting symbols. Figure 5 compares two such data sets taken before and after a rotor spin-up which changed ω_{rzd} from 48.54 to 51.74 rpm. The two data sets fall along the same curve although the data with the higher ω_{rzd} value appear to have slightly higher dedamping values. At the resonance peak, equation (67) from the Iorillo slosh model predicts a 12-percent difference between the data sets, while equation (73) from the time con-

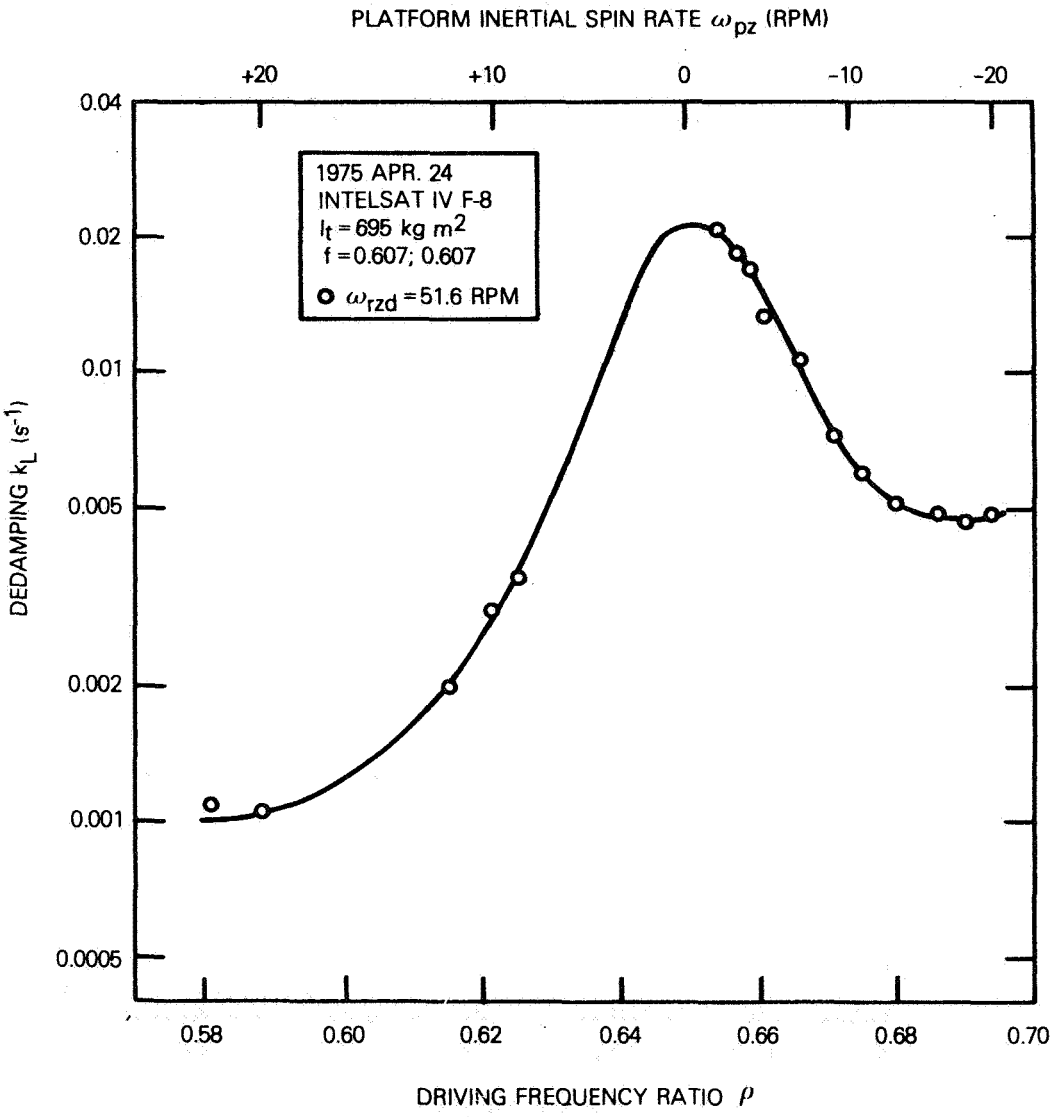

Figure 6. *Tank Liquid Dedamping Contribution for a 61-Percent Fill Fraction*

stant group predicts only a 6-percent difference. There is too much scatter in the data to decide between the two predictions.

Problems in the interpretation of the observed resonances

Before the in-orbit tests, *no* liquid resonance was expected within the range of frequency ratios tested. This opinion was based on ground measurements of the lowest mode natural frequency of the liquid in non-spinning spherical and conispheric tanks. Tests at COMSAT Laboratories

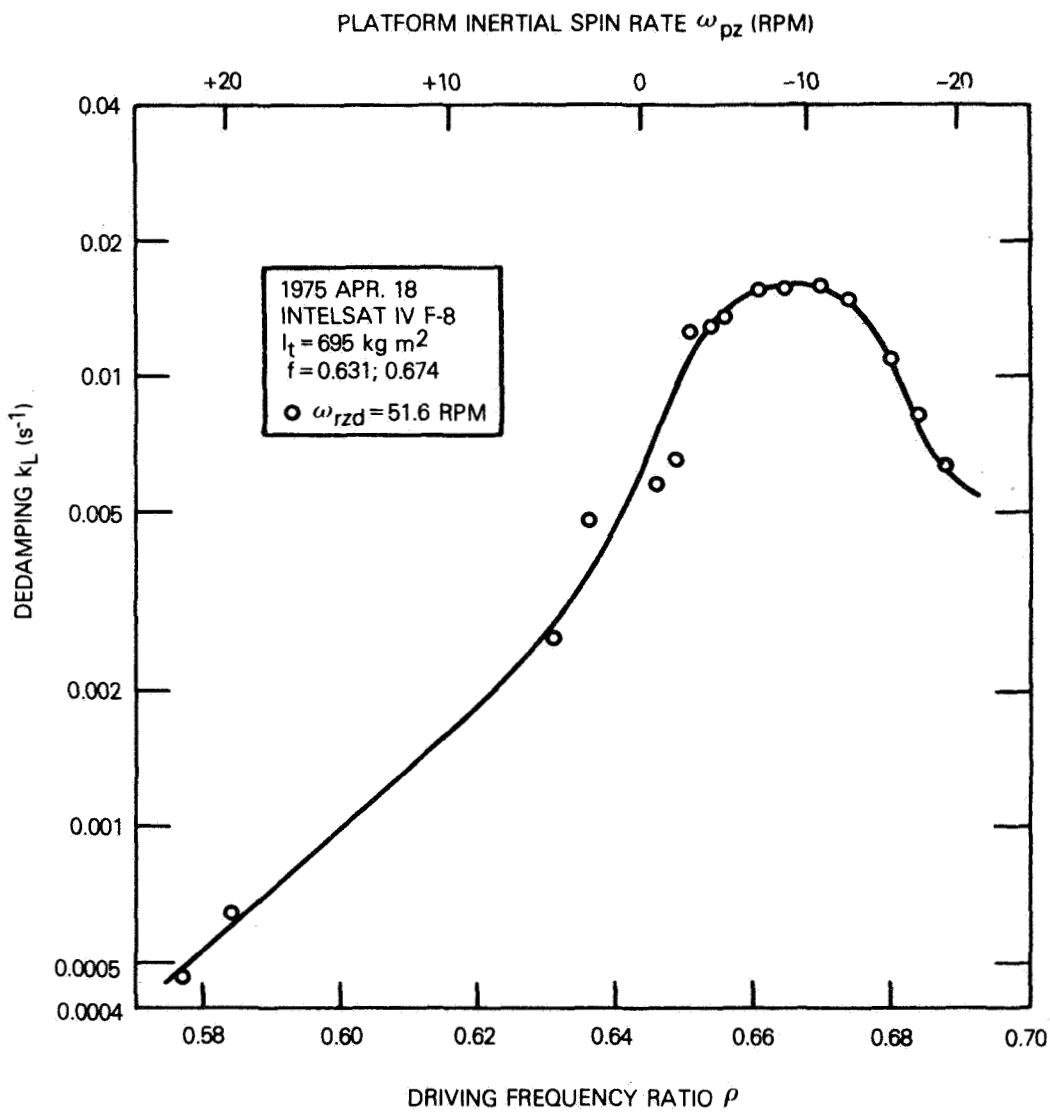

Figure 7. *Tank Liquid Dedamping Contribution for a 63.67-Percent Fill Fraction*

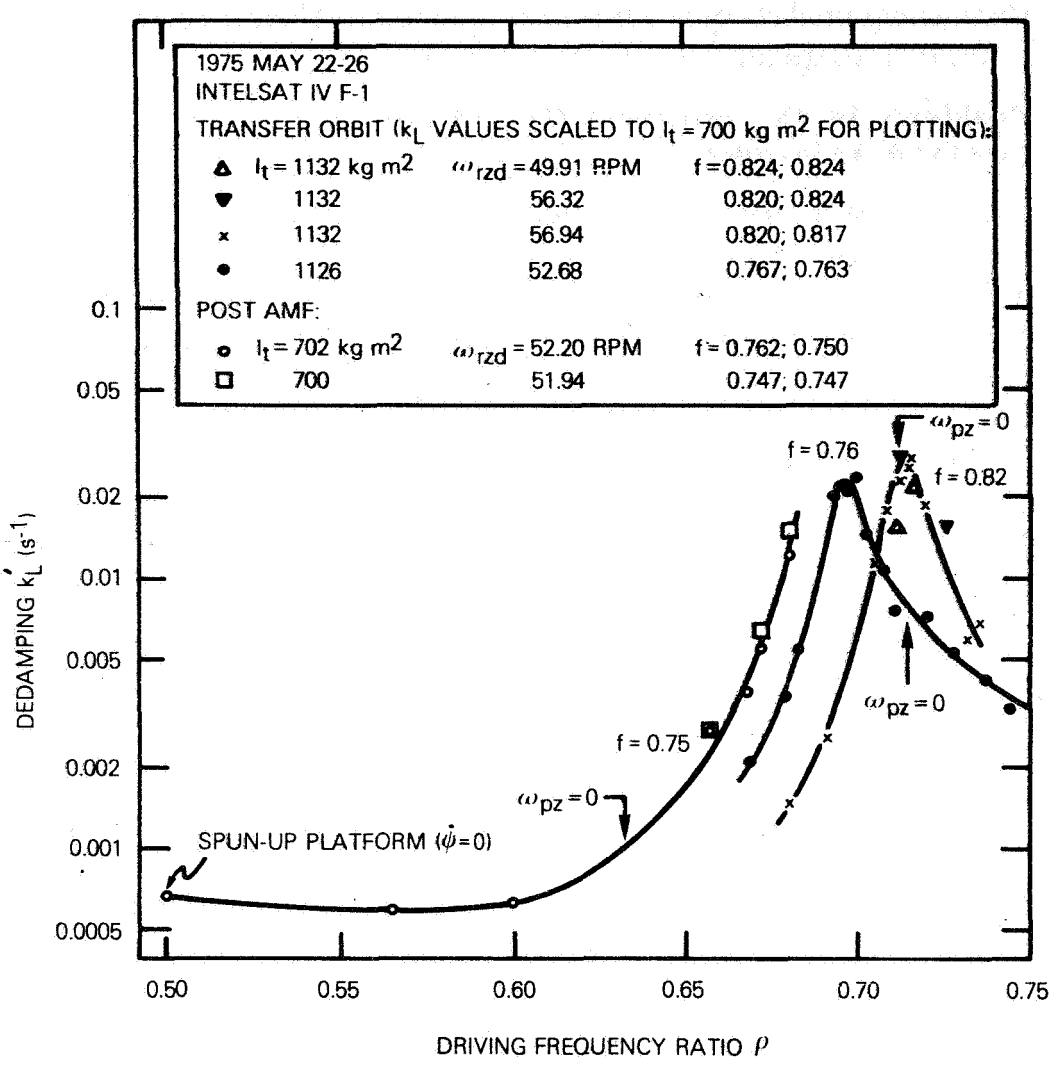

Figure 8. *Tank Liquid Dedamping Contribution for Three Different Fill Fractions Obtained During Launch Operations*

showed that the two tank geometries have the same natural frequency within 10 percent for a given fill fraction between 8 and 81 percent. These measurements indicated that the liquid resonance frequencies would always be much higher than the nutation frequency.

For small amplitudes, the lowest mode oscillation consists of liquid motion in the spherical tank section much like a rigid body undergoing a pendulum oscillation about an axis through the sphere center. This motion with a nearly planar free liquid surface is similar to the residual sloshing motion commonly observed in liquid containers such as water buckets and wine glasses. Because this is a pendulum-like motion, the

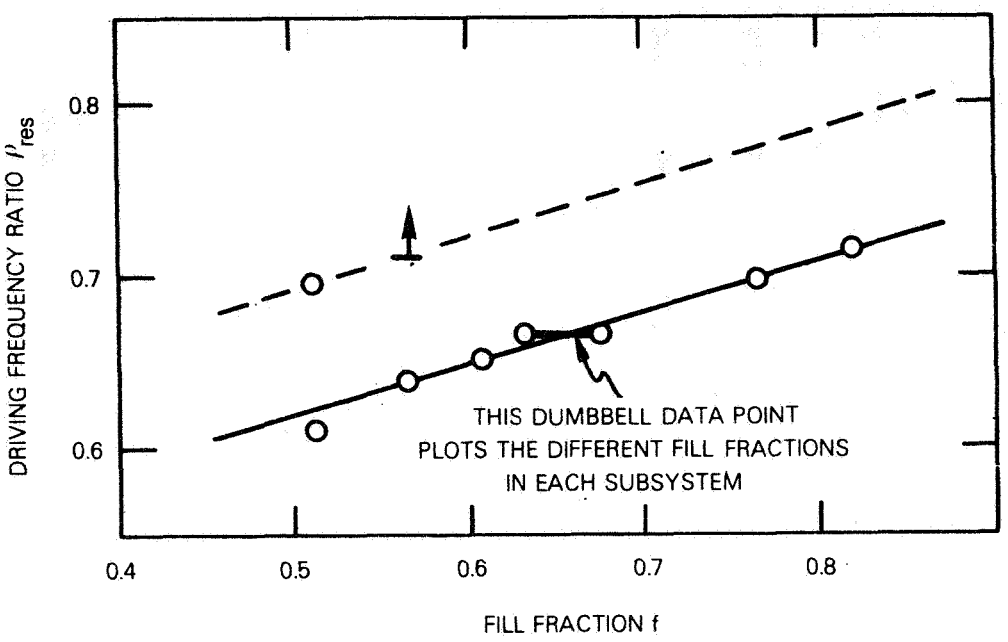

Figure 9. *Driving Frequency Ratio at an Anomalous Resonance vs Fill Fraction for the Conispheric Tanks*

ground measurements of natural frequency collected in Reference 7 can be scaled to in-orbit conditions by replacing the acceleration of gravity, g, in that figure with the appropriate centrifugal acceleration in the spacecraft tank. For longitudinal oscillations this acceleration is $\omega_{rz}^2 R_c$, where R_c is the distance from the bearing axis to the liquid mass center, while for transverse oscillations the effective acceleration is $\omega_{rz}^2 R_T$. The latter acceleration is smaller because, for transverse displacements from equilibrium, the mass center of the equivalent physical pendulum does not approach the bearing axis as rapidly as for longitudinal displacements. Indeed, for a pendulum pivot on the bearing axis ($R_T = 0$), transverse displacements keep the mass center at a constant distance from the bearing axis so there would be no centrifugal restoring force to produce oscillation. Table 3 compares the resulting predictions with the observed resonances for different fill fractions and shows that the predicted values are $\sim$3 times the observed values.

The fact that the predicted frequency ratio for a transverse resonance is roughly three times the observed frequency ratio has led to speculation that a liquid resonance at a multiple of the nutation frequency was excited through nonlinear effects. This superharmonic resonance hypothesis to explain the dedamping peaks can be dismissed by the following two argu-

TABLE 3. OBSERVED IN-ORBIT LIQUID RESONANCES AND PREDICTED LOWEST MODE NATURAL FREQUENCIES*

Parameters	Fill Fraction, f					
	0.512	0.564	0.607	0.631; 0.674 (unequal systems)	0.765	0.819
Ratio of Liquid Depth, h, in Spherical Section to Tank Radius, r	0.991	1.062	1.123	1.157; 1.219	1.356	1.444
Natural Frequency Parameter, $\Lambda_1(h/r) = \omega_d\sqrt{r/g}$ [7]	1.24	1.27	1.29	1.31; 1.34	1.42	1.48
Liquid Mass Center Distance from Bearing Axis for Spherical Section, R_c/r	3.00	2.96	2.92	2.91; 2.87	2.81	2.77
Predicted Natural Frequency Ratios:						
$\rho_{long} = \sqrt{R_c/r}\,\Lambda_1$ for Longitudinal Oscillation	2.15	2.18	2.21	2.23; 2.26	2.38	2.47
$\rho_{trans} = \sqrt{R_T/r}\,\Lambda_1$ for Transverse Oscillation	2.01	2.05	2.09	2.12; 2.16	2.30	2.40
Observed In-Orbit Ratio ρ_{res} for Anomalous Resonance	0.695; 0.610 (two resonances)	0.637	0.650	0.666	0.696	0.714
Predicted Value/Observed Value:						
ρ_{long}/ρ_{res}	3.1; 3.5	3.4	3.4	3.3; 3.4	3.4	3.4
ρ_{trans}/ρ_{res}	2.9; 3.3	3.2	3.2	3.2; 3.2	3.3	3.4

*The radius of the spherical tank section, $r = d_T/2 = 0.221$ m. The distance from the bearing axis to the tank sphere center, $R_T = 0.578$ m.

ments. First, an unpublished analysis by the author shows that, for an oscillating mass motion on the spacecraft in response to nutation, only the frequency component of the oscillation at the nutation frequency contributes to the dedamping. The tank liquid may undergo a large amplitude oscillation at its natural frequency due to a superharmonic resonance, but this oscillation is not at the nutation frequency and thus cannot produce a secular change in the nutation angle. Second, a careful analysis of several dozen nutation strip chart recordings shows that the observed nutation amplitude varies exponentially with time as given by equation (1).* Therefore,

$$\dot{\theta} = \frac{\theta}{\tau} \tag{74}$$

where τ is a constant. The time rate of change of the nutation angle is thus proportional to the nutation angle; *i.e.*, the damping and dedamping mechanisms are operating in their linear range and nonlinear effects are not important.

To illustrate the difficulty of using a liquid pendulum-motion resonance to explain the in-orbit data, it can be attempted to model the dedamping by a simple pendulum of length l_c pivoted at a point fixed in the rotor with the pendulum point mass positioned within the liquid volume. Such pendulum models have the desired property that, as in the case of liquids, their natural frequency, ω_n, is proportional to the rotor spin rate. For longitudinal oscillations,

$$\frac{\omega_n}{\omega_{rz}} = \sqrt{\frac{R_c}{l_c}} \tag{75}$$

where R_c is now the distance of the pendulum mass from the bearing axis. For transverse oscillations,

---

*Some small departures from an exponential fit to INTELSAT IV nutation data have been observed as follows. The amplitude for the first five cycles following a thruster pulse is often less than that predicted by an exponential fit, but this is attributed to an initial transient in the damper and liquid motions. The first few cycles are therefore excluded from the fit. The residuals from an exponential fit to the peaks of the following cycles sometimes show a systematic slow oscillation with period $\sim$30 s, but the amplitude is of the same order as the measurement accuracy so that this is not conclusive evidence for departure from an exponential variation.

$$\frac{\omega_n}{\omega_{rz}} = \sqrt{\frac{R_c}{l_c} - 1} \quad . \tag{76}$$

For the ratio ω_n/ω_{rz} to be equal to the observed dedamping resonance ratio of $\sim$0.66, longitudinal oscillations require $l_c \simeq 2.3\ R_c$; that is, the pendulum mass and pendulum pivot must be on opposite sides of the bearing axis. This is a physically unrealistic model. Transverse oscillations require $l_c \simeq 0.7\ R_c$; that is, the pendulum pivot is outside the tank near the bearing axis instead of near the tank center. This is also an unsatisfactory model.

Conclusions and suggestions for further investigations

The in-orbit dedamping measurements and the considerations of the previous subsection lead to the following conclusions: (a) over the range of ρ values tested, there are two anomalous resonance peaks; (b) their cause is unknown. It is highly desirable to discover the excitation mechanism that causes the anomalous resonances so that mathematical models can be constructed that would allow ground test results to be easily scaled to in-orbit conditions. Useful information could be obtained from a spinning test fixture such as the angular motion fixture described by Martin in Reference 8 (pp. 9–12) or the spinning air bearing fixture at Hughes Aircraft Co. (Reference 6, Chapter 3; also Reference 1, p. 75, Figure 7) since these spinning fixtures also exhibit anomalous liquid resonances. However, these fixtures must be instrumented to provide quantitative measurements of the actual motion of the liquid. A closed circuit television camera is sometimes mounted on the rotating test vehicle to view the liquid contained in a transparent tank. Such cameras have not proven useful in quantitative work because nonlinear effects are likely to be introduced by the large nutational motion usually required to give measurable liquid motion. Such cameras can give useful qualitative results, however.

The author has proposed that *liquid height gauges* be used to obtain quantitative measurements of the amplitude and phase of the rise and fall of points on the free liquid surface. Even coarse (10-percent) measurements could define the surface motion from which the mode of liquid oscillation (longitudinal, transverse, or other) at resonance could be deduced. The gauge proposed here is based on the electrical conductance between an electrical probe and the tap water used in place of hydrazine

as the tank liquid in ground tests. As shown in Figure 10, two bare electrical probes ~2 mm in diameter are required: one probe, called the ground probe, extends several centimeters below the liquid surface, while the second probe, called the surface probe, extends only 2 or 3 mm below the surface. The surface probe should be mounted no closer than 2 mm to the tank wall to prevent water drops from forming between the probe and the tank wall and giving erratic conductivity variations.

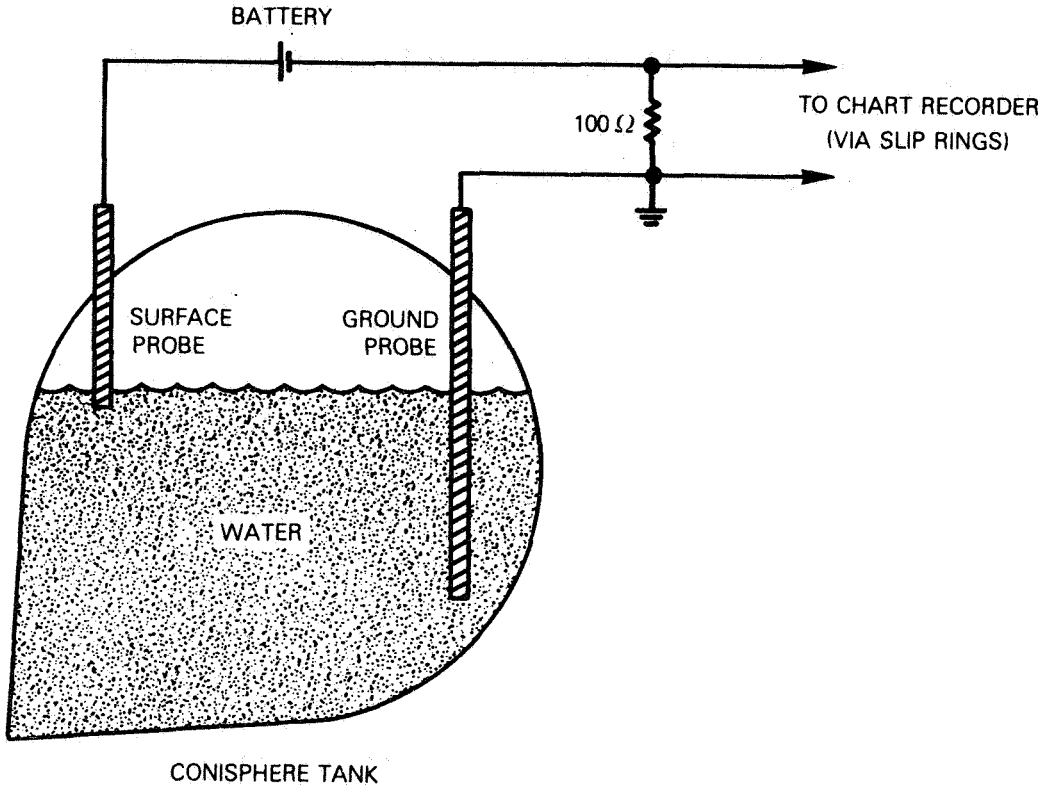

Figure 10. *Liquid Height Gauge Circuit for Liquid-Slosh Quantitative Measurements*

The electrical conductance of the water between the probes is of the order of $(10\ k\Omega)^{-1}$, and is largely independent of the distance between the probes. The liquid slosh measurements are based on the fact that this electrical conductance depends largely on the area of the surface probe in contact with the water. For a probe of uniform cross section, this area varies linearly with the depth of the surface probe in the water. Then, for the circuit shown in Figure 10, the electric current flowing between the probes varies linearly with liquid height as does the resulting voltage across the 100Ω signal resistor.

The voltage across the signal resistor thus reflects the changing height of the fluid at the surface probe due to liquid slosh. The surface motion should be restricted to ± 1 mm to ensure that the surface probe is always in the water, and to maintain a linear relation between voltage and surface height. Because of the small volume of each probe, several surface probes can be mounted at different places in the tank. These height gauges should be located so that different probes are sensitive to different modes of liquid slosh.

R. A. Curtis of COMSAT Laboratories has constructed and tested such a liquid height gauge. The apparatus gives satisfactory performance on the spinning test fixture described by Martin in Reference 8 (pp. 9–12). N. S. Lomas has used the fixture with a single height gauge and a television camera to look for resonances in a conispheric tank containing water at an 86-percent fill. A structural resonance limited the driving frequency ratio to values below 0.53, that is, to values far below the in-orbit resonance values. Liquid resonances associated with transverse and longitudinal oscillations were found for $\rho = 0.349$ and 0.407 respectively. These values are nearly one-half the resonance values of 0.72 and 0.80 predicted for $f = 0.86$ by the straight lines fit to in-orbit data in Figure 9. The liquid was oscillating at the driving frequency. No firm conclusions about these newly observed resonances can be made because the height gauge showed many large-amplitude harmonics of the driving frequency whose presence is unexplained.

Finally, experimental and theoretical consideration should be given to a possible *swirl oscillation* of the liquid, which is explained as follows. The body of the liquid, if treated as a rigid body sliding within a spherical tank, can oscillate with three degrees of freedom about three mutually orthogonal axes. Two of these axes are "parallel" to the equilibrium free liquid surface and correspond to the usual longitudinal and transverse oscillation of the liquid as a physical pendulum. The third axis is normal to the free liquid surface at the surface center and is the axis for swirl motion of the liquid. For a non-spinning tank on the ground, a displacement of the liquid about the swirl axis results in no restoring torque on the liquid; no swirl oscillation occurs in this case. On a spinning satellite, however, the equilibrium free liquid surface is a portion of a cylinder whose axis is the spin axis. A rigid-body displacement of the liquid about the swirl axis results in a restoring torque due to centrifugal forces which attempt to bring the cylindrical surface back into alignment with the *instantaneous* spin axis. The natural frequency of the resulting oscillation about the swirl axis may well correspond to an observed anomalous

resonance. This swirl oscillation would be driven by spacecraft nutation because the direction of the spin axis about the swirl axis oscillates with time.

Acknowledgments

The INTELSAT IV *liquid slosh tests were a cooperative effort by many people at* COMSAT. *The initial analyses that led to the tests were performed by L. B. Ricks and A. A. Satterlee of* COMSAT *and J. O. Salvatore of Hughes Aircraft Co. L. R. Dest of* COMSAT *helped reduce most of the nutation strip chart recordings and suggested many improvements to the text of this paper.*

References

[1] J. T. Neer, "INTELSAT IV Nutation Dynamics," *Progress in Astronautics and Aeronautics*, Vol. 33, 1974, pp. 57–84; AIAA Paper No. 72-537.

[2] Special INTELSAT IV Issue, *COMSAT Technical Review*, Vol. 2, No. 2, Fall 1972, pp. 271–576.

[3] G. A. Haines and C. T. Leondes, "Eddy Current Nutation Dampers for Dual-Spin Satellites," *Journal of the Astronautical Sciences*, Vol. 21, 1973, pp. 1–25.

[4] G. D. Gordon, G. R. Huson, and V. J. Slabinski, "Blocking Bubbles in the INTELSAT IV Fuel Lines," *COMSAT Technical Review*, Vol. 4, No. 2, Fall 1974, pp. 499–506.

[5] A. J. Iorillo, "Nutation Damping Dynamics of Axisymmetric Rotor Stabilized Satellites," American Society of Mechanical Engineers Winter Meeting, Chicago, Illinois, November 1965, *ASME Miscellaneous Papers*, ESL Paper No. 238, pp. 11–19.

[6] J. T. Neer and J. O. Salvatore, "Fuel Slosh Energy Dissipation on a Spinning Body," Report SCG 20047R, Hughes Aircraft Co., February 1972.

[7] Sandor Silverman and H. Norman Abramson, "Lateral Sloshing in Moving Containers," *The Dynamic Behavior of Liquids in Moving Containers*, H. N. Abramson, ed., NASA SP-106, 1966, Ch. 2, p. 52, Figure 2.28.

[8] E. R. Martin, "Experimental Investigations on the Fuel Slosh of Dual-Spin Spacecraft," *COMSAT Technical Review*, Vol. 1, No. 1, Fall 1971, pp. 1–20.